



ACADÉMIE
DES SCIENCES
INSTITUT DE FRANCE

Comptes Rendus

Mécanique


Said Derbane, Mouloud Mansouri, Salah Messast
and Aboulghit El Malki Alaoui

**On the behavior of a granular soil deposit subjected to horizontal vibration. A
discrete element modeling**

Volume 353 (2025), p. 321-338

Online since: 27 January 2025

<https://doi.org/10.5802/crmeca.282>

 This article is licensed under the
CREATIVE COMMONS ATTRIBUTION 4.0 INTERNATIONAL LICENSE.
<http://creativecommons.org/licenses/by/4.0/>



*The Comptes Rendus. Mécanique are a member of the
Mersenne Center for open scientific publishing*
www.centre-mersenne.org — e-ISSN : 1873-7234



Research article / *Article de recherche*

On the behavior of a granular soil deposit subjected to horizontal vibration. A discrete element modeling

Comportement d'un dépôt de sol granulaire soumis à une vibration horizontale : Modélisation par éléments discrets

Said Derbane^{®,* ,a}, Mouloud Mansouri^{® ,b}, Salah Messast^{® ,a} and Aboulghit El Malki Alaoui^{® ,c}

^a Department of Civil Engineering, LMGHU Laboratory, University of 20 August 1955 Skikda, BP 26, 21000, Skikda, Algeria

^b Department of Civil Engineering, University of Ferhat Abbas Sétif 1, Setif 19000, Algeria

^c ENSTA Bretagne, IRDL, UMR 6027, CNRS, 29806 Brest, France

E-mail: derbane_said@yahoo.fr (S. Derbane)

Abstract. This paper presents an analysis of the behavior of a non-cohesive granular material deposit excited at its base by a horizontal harmonic vibration. The analysis is carried out numerically by means of a 2D discrete element model. The performed simulations highlighted some aspects of vibration behavior in non-cohesive deposits, such as the shape of the vertical profile of the displacement, notably in the case of large displacements. The analysis particularly focused on the amplification of the movement at the free surface of the deposit, as well as its dependence on some parameters such as the excitation frequency and the excitation amplitude of the deposit confinement. The obtained results showed that the behavior of the deposit following the change in the excitation frequency is similar to the case of an elastic deposit excited by a harmonic displacement at the base, i.e. the Dynamic Amplification Factor (DAF) initially increases with the frequency increase, it reaches a peak of resonance then it decreases. The resonance frequency estimated from this analysis is close to the fundamental frequency for low excitation amplitudes, but becomes smaller as the excitation amplitude increases. On the other hand, for a fixed frequency, increasing the amplitude of the excitation induces greater amplification. It has been shown that this increase results from the degradation of the shear modulus due to the increase in the level of involved shear strain. Therefore, unlike elastic deposits, for non-cohesive granular deposits, increasing strain leads to a degradation of the shear modulus, resulting in a downward shift of the resonance frequency and can induce a significant increase in amplification. The confinement of the deposit is achieved by increasing the gravitational acceleration; it has been shown that increased confinement makes the deposit stiffer, and therefore reduces the amplification of the introduced movement.

Résumé. Cet article présente une analyse du comportement d'un dépôt de matériau granulaire non cohésif soumis à une vibration harmonique horizontale appliquée à sa base. L'analyse est réalisée numériquement à l'aide d'un modèle bidimensionnel basé sur la méthode des éléments discrets. Les simulations effectuées ont mis en évidence certains aspects du comportement vibratoire des dépôts non cohésifs, notamment

*Corresponding author

la forme du profil vertical du déplacement, en particulier dans le cas de grands déplacements. L'analyse s'est particulièrement concentrée sur l'amplification du mouvement à la surface libre du dépôt, ainsi que sur sa dépendance à certains paramètres tels que la fréquence et l'amplitude de l'excitation ou encore le confinement du dépôt.

Les résultats obtenus montrent que le comportement du dépôt face à la variation de la fréquence d'excitation est similaire à celui d'un dépôt élastique soumis à un déplacement harmonique à sa base. Plus précisément, le facteur d'amplification dynamique (DAF) augmente initialement avec la fréquence, atteint un pic de résonance, puis diminue. La fréquence de résonance estimée dans cette analyse est proche de la fréquence fondamentale pour de faibles amplitudes d'excitation, mais devient plus basse à mesure que l'amplitude augmente. Par ailleurs, pour une fréquence donnée, l'augmentation de l'amplitude de l'excitation engendre une amplification plus importante. Il a été démontré que cette augmentation résulte de la dégradation du module de cisaillement due à une augmentation du niveau de déformation en cisaillement. Contrairement aux dépôts élastiques, pour les dépôts granulaires non cohésifs, l'augmentation de la déformation conduit à une dégradation du module de cisaillement, entraînant un décalage vers le bas de la fréquence de résonance et pouvant induire une amplification significative.

Le confinement du dépôt est simulé par une augmentation de l'accélération gravitationnelle. Il a été montré qu'un confinement accru rend le dépôt plus rigide, ce qui réduit l'amplification du mouvement introduit.

Keywords. Sand deposit, Behavior of a granular soil, Discrete element method, Shear wave, Propagation.

Mots-clés. Dépôt de sable, Comportement d'un sol granulaire, Méthode des éléments discrets, Onde de cisaillement, Propagation.

Manuscript received 12 June 2024, accepted 19 December 2024.

1. Introduction

Seismic wave propagation from the bedrock to the free ground surface depends strongly on the nature of the traversed soil layers. In particular, it is known that stiffness and damping of these layers have significant effects on the transmission of the motion. For granular soils these two properties i.e. stiffness and damping depend on the applied movement characteristics such as amplitude and frequency, as well as on certain soil state parameters, such as confining and density states. The classical methods used in the analysis of movement transmission and its amplification from the bedrock to the surface are usually based on continuum mechanics. These methods work well for cohesive soils, however for granular soils, given the discontinuous nature of the material, discrete element modeling could provide more understanding of the involved mechanisms.

In the context of this modeling approach, transient wave propagation in granular materials was studied using a discrete element model by Martin *et al.* [1], three particular cases were investigated including dry cohesionless material, elastic cemented particulate media and fluid saturated granular material, the results of this study indicated that the wave velocity depends upon the stiffness of the interparticle contacts and the distribution of branch vectors along the propagation direction. Furthermore, it is shown that the attenuation of the wave amplitude depends on the number of branch vectors in the propagation direction. The influence of force chains on the wave scattering and attenuation in granular soils was also studied by Peters and Muthuswamy [2]. As part of a study on the instabilities of force chains, Campbell [3] treated the destabilizing effect of wave propagation using discrete element modeling. Zamani and El Shamy [4] have carried out an investigation of the vertical propagation of a shear wave in a granular deposit through discrete element modeling, they studied the change of the shear modulus and the damping ratio for low frequencies. The properties extracted from the DEM simulations were used to calculate the deposit response assumed as a continuum with linear viscoelastic behavior using the SHAKE software. The obtained results were then compared to those of the

DEM modeling. Ning *et al.* [5], after developing an appropriate method for measuring wave velocity in a discrete element model, have studied the effects of particle size and elastic properties on the wave propagation velocity. O'Donovan *et al.* [6] have conducted an experimental study on a soil model in a cubical cell, they then compared the results with both discrete element (DEM) simulations and continuum modeling. In their study, they used point source transmitters and receivers in order to assess the shear and compression wave velocities in the samples, from which some of the elastic moduli can be deduced. As a result, a satisfactory agreement between experimental observations and DEM simulations is confirmed. Recently, Arran and co-authors [7] modeled the flow of spherical particles on a rough inclined base. By comparison with their experimental results on physical models dealing with seismic waves emitted by granular flows [8, 9] they highlighted the effect of velocities of basal particle, which are difficult to measure experimentally, on the flow properties. In order to better understand how the dynamic load affects the evolution of the microstructure and the whole granular assembly behavior, Longlong and Shunhua [10] proposed a criterion to recognize the major propagation path of dynamic load in 2D granular materials, called the "dynamic force chain". This analysis showed that the spatial distribution of dynamic force chains in the indentation of granular materials provides a direct measure of dynamic load diffusion. It is demonstrated that the statistical evolution of dynamic force chains has a strong correlation with the indentation behaviors. Besides, discrete element modeling of wave propagation in saturated granular materials has also received interest, particularly in the context of the study of sand liquefaction phenomenon under seismic vibrations [11–13].

Despite all these studies, movement propagation in granular soils still has many unclear behavioral aspects. Indeed, for these soils, deformation is particularly related to intergranular slips, which themselves depend on several parameters such as the strain amplitude, the vibration frequency, the confining pressure, etc. Hence, these complex aspects deserve to be subjected to more analysis. This work consists of an analysis of the behavior of a non-cohesive granular deposit subjected to dynamic excitation at its base using a 2D discrete element model. The exciting motion is harmonic with a controlled amplitude and frequency. We particularly aim to highlight and analyze some involved features, such as the movement amplification at the free surface and its dependence on the frequency and amplitude of excitation as well as the deposit confinement. We also show the macroscopic behavior of the deposit during large displacements or near the resonance.

2. Discrete element modeling

The discrete element method used in this work was first initiated by Cundall in 1992 [14] and is based on molecular dynamics. It models granular materials at the micromechanical scale using independent elements. The grains of the material interact with each other through contact forces that are calculated through simple models based on a slight overlap of the grains [15, 16]. It is assumed that the global deformation of the medium is mainly due to the relative movements of the grains considered as rigid bodies [17, 18]. Because of their simplicity and the savings in calculation time they involve, circular element shapes are still the most widely used.

The movement of each grain i is governed by the following Newton's second law, which allows to obtain the accelerations of the grains.

$$\left\{ \begin{array}{l} m_i \ddot{\vec{x}}_i = \sum_j \vec{F}_{ij}^{\text{contact}} + m_i \vec{g} \\ I_i \ddot{\vec{\varphi}}_i = \sum_j \vec{M}_{ij}^{\text{contact}} \end{array} \right. \quad (1)$$

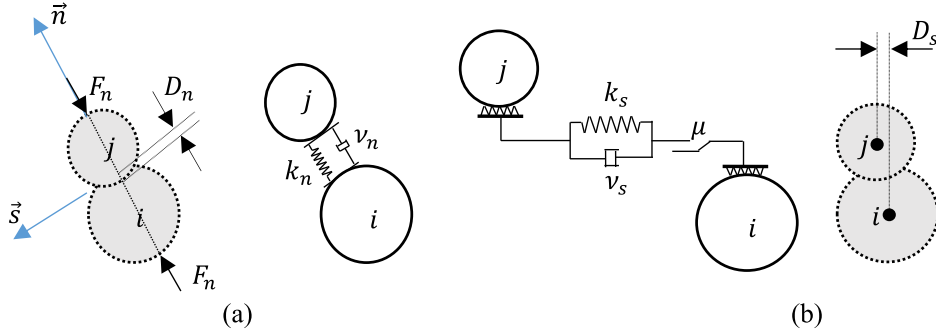


Figure 1. (a) Normal force model. (b) Shear force model.

with \ddot{x}_i and $\ddot{\varphi}_i$ represent respectively the translational and rotational accelerations of the grain i , m_i and I_i are the mass and the moment of inertia respectively, $\vec{F}_{ij}^{\text{contact}}$ is the interaction force applied by a grain j in contact with grain i , \vec{g} is the acceleration due to gravity and $\vec{M}_{ij}^{\text{contact}}$ is the torque with respect to the center of gravity of grain i applied by the contact forces $\vec{F}_{ij}^{\text{contact}}$.

Contact forces are decomposed into a normal component \vec{F}_n and a tangential component \vec{F}_s contained in the plane tangent to the grain at the point of contact [19]. In this work, the normal contact force is computed through the viscoelastic model (Figure 1a) as:

$$\vec{F}_n = (-k_n D_n - v_n V_n) \cdot \vec{n} \quad (2)$$

where k_n is the elastic constant, v_n is the viscous damping constant, V_n is the normal velocity and D_n is the overlap of the two grains i and j , defined geometrically by:

$$D_n = \|\vec{x}_j - \vec{x}_i\| - r_i - r_j \quad (3)$$

in which r_i and r_j are the radii of grains i and j .

The tangential contact force (\vec{F}_s) is computed through a viscoelastic model with friction (Figure 1b) as:

$$\vec{F}_s = \min(k_s D_s + v_s V_s, \mu_d F_n) \vec{s} \quad (4)$$

where k_s is the tangential stiffness, v_s the viscous damping coefficient, μ_d is the inter-particle coefficient of friction, D_s is the grain deformation due to shear force, V_s is the tangential velocity of grain j with respect to grain i and \vec{s} is the tangential unit vector as indicated in Figure 1a.

The duration of a contact between two grains (t_c) is equal to the natural half-period of the equivalent oscillator. Using this contact force model, this half-period is equal to:

$$t_c = \pi \sqrt{\frac{m_{\text{eff}}}{k_n}} \quad (5)$$

It is crucial in practice to consider this contact period t_c . In fact, the integration of the movement equations is only stable if the integration time step Δt is sufficiently small in comparison to t_c , i.e. the evolution of the contact should be accurately described. In practice, in order to prevent certain instabilities, the integration time step Δt is taken as [19]:

$$\Delta t_{\text{max}} \approx 0.1\pi \sqrt{\frac{m_{\text{eff}}}{k_n}} \quad (6)$$

where m_{eff} is the smallest effective mass in the system.

In order to account for the damping of the rolling motion of natural grains, a rolling resisting torque is incorporated in the model. This torque is calculated by placing the normal force off-center of the contact, such eccentricity is adjusted to reduce or increase rolling resistance.

It should be noted that in order to obtain quantitative results comparable to experimental ones, a calibration of the model parameters is necessary. However, for a phenomenological analysis such as in our case, these parameters are usually selected in such a way as to save computation time without departing from the normal behavior of the model.

3. Analytical solution of wave propagation in a viscoelastic deposit

For some mechanical and/or movement conditions where the deposit can be assumed as a continuum with elastic damped behavior, the equation governing the propagation of a horizontal harmonic displacement (u) in the vertical direction (z) is given by [20] as:

$$\frac{1}{c^2} \frac{\partial^2 u}{\partial t^2} = \frac{\partial^2 u}{\partial z^2} + \frac{2\xi}{\omega} \frac{\partial^3 u}{\partial t \partial z^2} \quad (7)$$

where c is wave propagation velocity, ξ is the hysteretic damping ratio and ω is the circular frequency of the movement. For a deposit of thickness h resting on an oscillating bedrock, the final solution of this equation is presented in [20] as:

$$\begin{aligned} \frac{A \cdot u(z, t)}{u_0} = & \cosh(ph) \cos(qh) \cosh(pz) \cos(qz) \sin(\omega t) \\ & + \sinh(ph) \sin(qh) \sinh(pz) \sin(qz) \sin(\omega t) \\ & + \cosh(ph) \cos(qh) \sinh(pz) \sin(qz) \cos(\omega t) \\ & - \sinh(ph) \sin(qh) \cosh(pz) \cos(qz) \cos(\omega t) \end{aligned} \quad (8)$$

with A , p and q are calculated from equations:

$$\begin{aligned} A &= \cosh^2(ph) - \sin^2(qh) \quad (9) \\ (ph)^2 + (qh)^2 &= \frac{(\pi^2/4)(\omega^2/\omega_1^2)}{1 + 4\xi^2} \quad \text{and} \quad (ph)(qh) = \xi \frac{(\pi^2/4)(\omega^2/\omega_1^2)}{1 + 4\xi^2} \quad (10) \end{aligned}$$

The fundamental frequency of the deposit being the first resonance frequency for very low damping, it is given by:

$$\omega_1 = \frac{\pi c}{2h} \quad (11)$$

This solution indicates that for a harmonic excitation, the displacement of any point of the deposit is harmonic. In addition, it states that the shape of the displacement, i.e. the plot of the displacement versus of the depth at a given time, depends on the excitation frequency. As examples, Figure 3 shows the displacement shapes for a deposit excited at its base by a harmonic displacement of amplitude u_0 and with excitation frequencies $\omega/\omega_1 = 0.42$ and $\omega/\omega_1 = 1.12$. For these examples, the damping ratio is set to $\xi = 8\%$. Note that the system's damping ratio can be estimated from the dynamic amplification factor at resonance as shown below.

This figure shows that for an excitation frequency lower than the fundamental frequency, the displacement profile has the shape of the first natural oscillation mode (Figure 3a). However, when the excitation frequency exceeds the fundamental frequency, the second mode shape appears by the formation of a zero-displacement node at a specific height that rises from the base. This height increases with the increase in the excitation frequency (see Figure 2b) until the second natural frequency is reached, then the shape of the third mode appears and so on.

In this study, we define the dynamic amplification factor at the top (i.e. the free surface) as $DAF = u_s/u_0$, where u_s and u_0 are the displacement amplitudes at the free surface and at the base respectively. Using the displacement solution (Equation (8)), the DAF is plotted in Figure 3 in terms of the frequency ratio (ω/ω_1) ranging from 0 to 1.12 and for damping ratios of 5%, 10% and 15%.

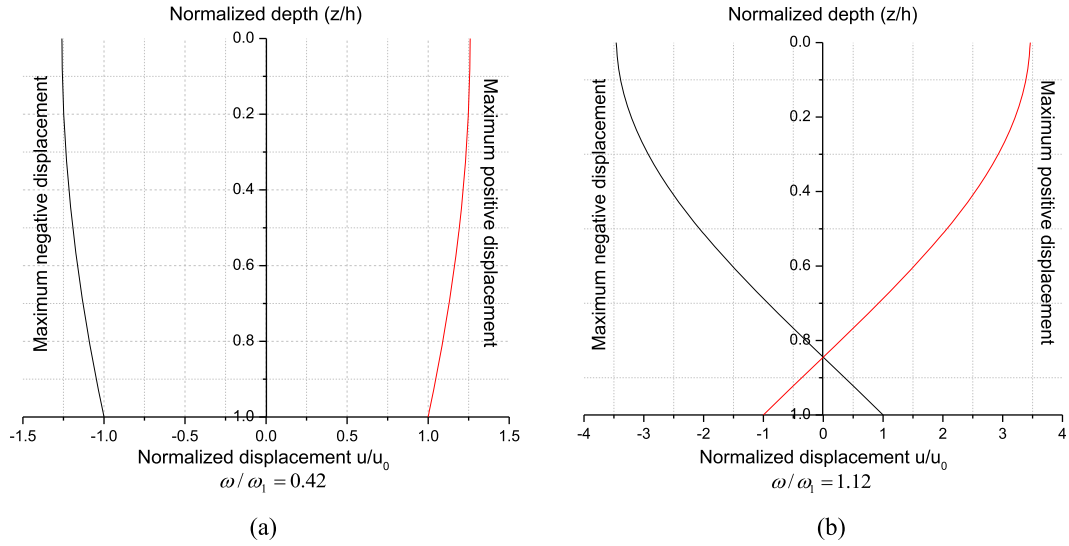


Figure 2. Normalized displacements of analytical solution for two different excitation frequencies.

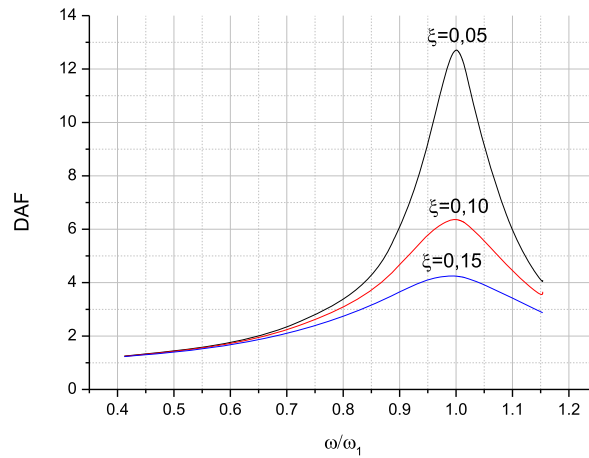


Figure 3. Dynamic Amplification Factor at the deposit’s free surface (DAF) in terms of the frequency ratio (ω/ω_1) damping ratios: 5%, 10% and 15%.

This figure clearly shows the typical evolution of amplification against the excitation frequency increasing. The DAF increases starting from 1 for low frequencies, it reaches a maximum value at the first resonance frequency then it decreases. The maximum DAF value occurring at resonance is inversely proportional to the damping ratio, it can be approximated for low damping ratios by $DAF_{max} \approx 2/\pi\xi$ [20]. It is worth noting that for common dampings, the resonance occurs at frequencies very close to the fundamental frequency.

4. Details of the numerical model of wave propagation

In the present work, an analysis of the vertical propagation of a shear wave in a sand deposit is carried out using 2D discrete element modeling, the used model is implemented in a C++

Table 1. Model parameters

Parameters	Value
Number of grains	5000
Grains radii r_i	1.00×10^{-3} to 2.00×10^{-3} m
Density G_s	2600 kg/m ³
Normal intergranular stiffness k_n	1.2×10^6 N/m
Shear intergranular stiffness k_s	9.6×10^5 N/m
Intergranular friction coefficient μ	0.5

code. In a first step, a dense deposit is built by pluviation under gravity on a horizontal rigid plateau (considered as a bedrock), with introducing periodic boundaries to model an infinite layer in the horizontal direction. After stabilization, the positions of the grains of the deposit are stored to become the reference positions for displacements. Next, the deposit is subjected to a horizontal vibration through the supporting bedrock, while the upper surface of the deposit is kept free. In order to ensure good transmission of movement to the deposit, the bedrock is roughened by bonding the lowest deposit grains to it. Therefore, these grains undergo the same imposed bedrock displacement. In order to describe the response, the deposit is divided into a number of layers for which the average grain displacements are monitored during the excitation.

The properties of the grains as well as the micromechanical parameters used in the computation of the intergranular contact forces are presented in Table 1.

The width of the deposit (i.e. the period) is initially set to 2 m, the resulting height for the used number and size of the grains is about 0.54 m. Figure 3 shows the obtained sand deposit model after pluviation with the different boundary conditions as well as the bonded chain of grains called “excitation chain”. The subdivision of the deposit into control layers is also illustrated in the same figure.

In this work, the applied excitation is a harmonic horizontal displacement of specified amplitude and frequency $u(t) = u_0 \sin(\omega t)$, where u_0 is the amplitude and ω is the circular frequency. In order to avoid the transient response disturbances, the excitation is applied in three stages according to the same idea presented in reference [4]. In the first step, the amplitude is gradually increased from zero to the selected steady-state vibration amplitude. In the second stage, the amplitude is maintained constant to produce a steady state oscillation. Finally, in the third stage the amplitude is decreased from the steady-state amplitude until zero. In the following simulations, the durations of the three stages are respectively set to 4.5 s, 6 s and 1.5 s. In this way, the transient response should become almost attenuated in the steady-state oscillation phase. The results that will be discussed below, essentially belong to this later phase. The deposit is divided into 10 control layers and the recorded displacement is the average displacement over all grains belonging to the layer.

5. Simulation results and discussion

5.1. Displacement time history and movement amplification

In this simulation, the parameters of the exciting displacement are set to $u_0 = 4 \times 10^{-4}$ m and $\omega = 25$ rad/s. In the first stage (i.e. from 0 to 4.5 s), the displacement amplitude is increased proportionally to time from zero until 4×10^{-4} m. Then, maintained at the same level for 6 s and finally decreased gradually to reach zero during 1.5 s. Figure 4 shows the displacement time history at the bedrock (Figure 5a) and at the top layer of the deposit (Figure 5b).

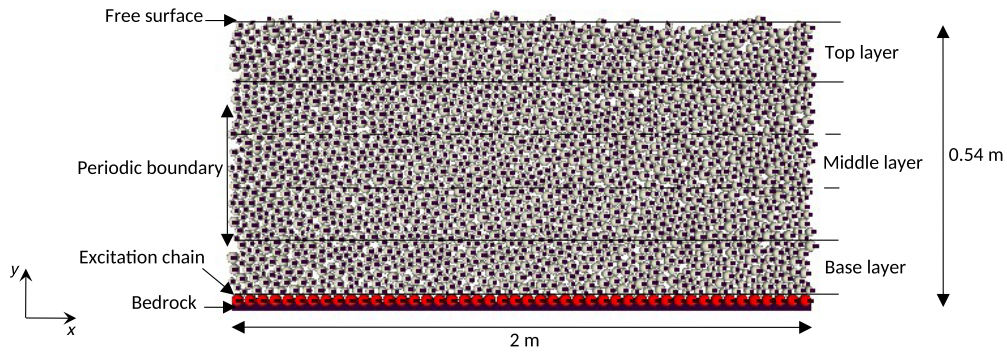


Figure 4. Illustration of the sand deposit's model, boundary conditions and subdivision into a number of monitoring layers.

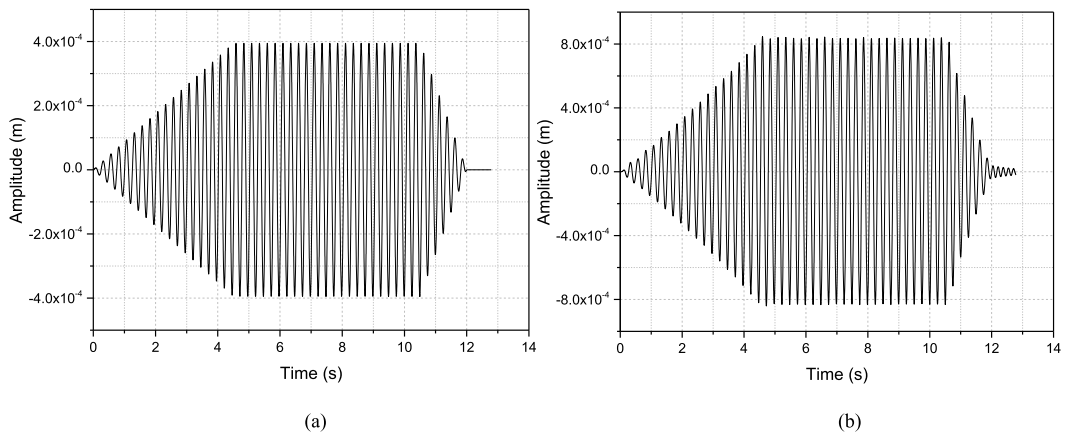


Figure 5. Displacement time history, (a) at the bedrock (excitation), (b) at the top layer of the deposit.

These figures clearly show the different phases of the movement at the bedrock and at the top layer (which represents approximately the surface of the deposit). Figure 4b shows that the amplitude at the deposit's surface in the steady state phase is almost constant, i.e. the effect of the transient response disappears in this phase. The comparison of the two displacement plots (Figures 5a, b) in the steady state phase, shows that the introduced displacement at the bedrock (excitation) having an amplitude of 0.4 mm is amplified in the top layer where the amplitude becomes about 0.85 mm. Besides, Figure 4b shows that the deposit experiences a free elastic damped oscillation after ending the excitation (i.e. after $t = 12$ s).

The amplification of the movement in the bulk of the deposit is illustrated in Figures 5a, b. The first shows a part of the steady state response ($7 \text{ s} \leq t \leq 8 \text{ s}$) at the base, the middle and the top layers, and the second presents the vibration amplitude versus the layer's height from the bedrock (y -coordinate).

These figures indicate that the movement amplification increases from the base up to the top layer. On the other hand, Figure 6b shows that the displacement profile has the characteristic shape of the first mode of vibration; this reveals that the excitation frequency is lower than the first resonance frequency of the deposit.

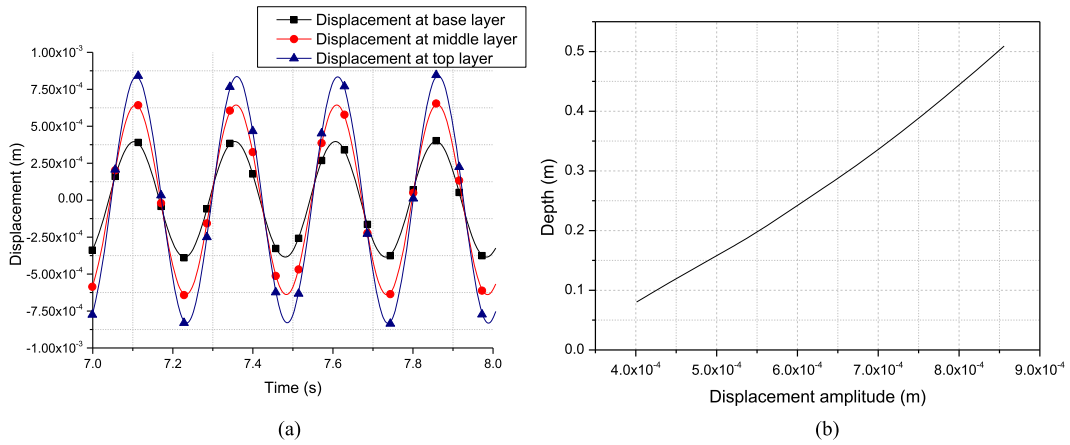


Figure 6. (a) Displacement time history for steady state oscillation at three different depths. (b) Displacement amplitude versus the layer's height from the bedrock during steady state oscillation.

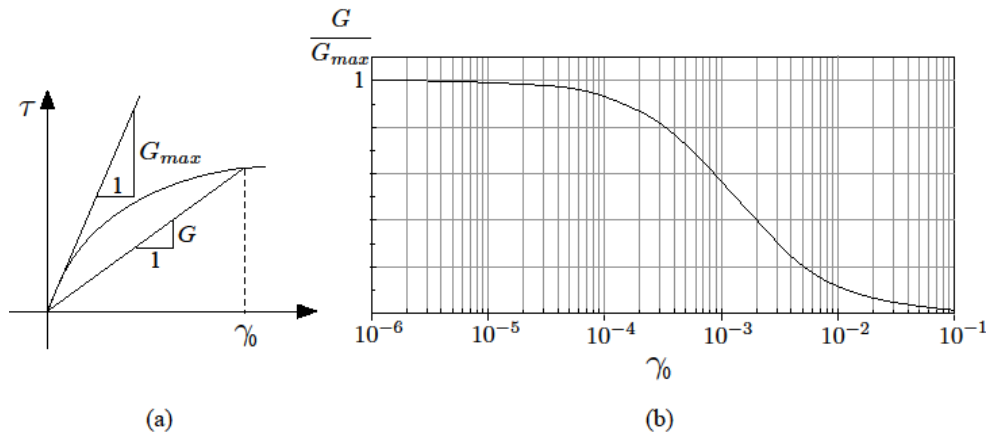


Figure 7. (a) Illustration of the degradation of the shear modulus with increasing applied strain. (b) Shear modulus degradation curve versus the strain level [21].

5.2. Fundamental frequency of the deposit

Soils are known for their non-linear mechanical behavior, their shear modulus degrades when the level of strain involved increases, as shown in Figure 7a. In this figure, G_{max} is the small strain shear modulus and G is the modulus corresponding to a specified strain γ . Figure 7b shows the degradation curve of G in terms of the involved level of strain (γ_0) according to reference [21]. It is clear that G_{max} corresponds to strains approximately smaller than 10^{-5} .

The fundamental frequency is defined as the first natural frequency of a small strain (pseudoe-lastic) oscillation. To obtain this frequency, we subjected the deposit to a harmonic vibration in the same way described above, with the amplitude $u_0 = 4 \times 10^{-4}$ m and the frequency of 25 rad/s. The fundamental frequency of the deposit is taken as the frequency of free vibration remaining after the end of the excitation. Figure 8 presents a zoom of the time history of displacements corresponding to the free vibration phase (after the end of excitation) at different depths of the

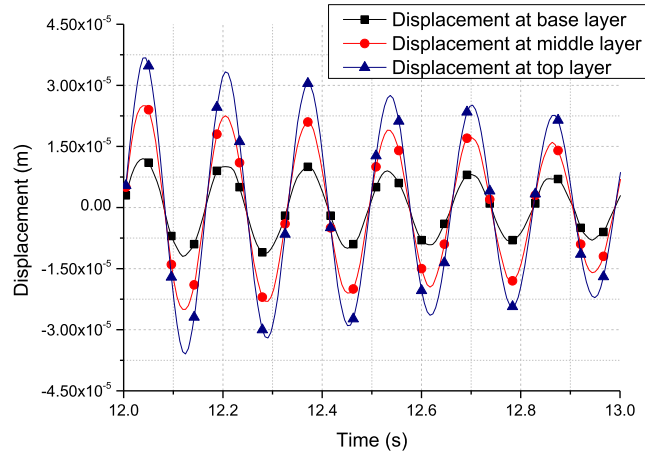


Figure 8. Zoom of time history response at different depths for free vibration phase.

deposit. This figure shows that the displacements are harmonic and without a phase offset for the different depths, which corresponds to the oscillation shape of the fundamental mode. The fundamental period can be estimated from the displacement plot, it is about $T = 0.166$ s. Hence, the fundamental frequency is $\omega_1 = 2\pi/T = 37.82$ rad/s.

For an elastic oscillation of the deposit, the shear wave velocity can be calculated from the fundamental period through the expression $c = 4h/T$ [20], hence for our deposit $c = 12.91$ m/s.

Besides, it could be noted that the wave propagation velocity for this model is lower than the characteristic velocities of natural soils. This is reasonable due to the low intergranular stiffness deliberately adopted in the model in order to reduce the calculation time. However, it appears that this wave velocity has a negligible effect on the phenomenological aspects of the response. O'Donovan *et al.* [6], following their simulations on wave propagation in granular media, indicated that the change in intergranular stiffness changes the propagation velocity but has no noticeable effect on the nature of the response.

5.3. Influence of the excitation frequency on the response of the deposit

In order to show the excitation frequency effect on the deposit's response, several simulations are performed for frequencies ranging from 10 to 40 rad/s, while the excitation amplitude is set to $u_0 = 4 \times 10^{-4}$ m. Figure 9 shows the time history of displacements during the steady state excitation stage at the bedrock and at the top layer of the deposit for frequencies of 10 and 20 rad/s. It can be noted that for the frequency of 10 rad/s, there is no movement amplification at the top layer, thus the deposit exhibits a behaviour of a rigid body that follows the bedrock's displacement. However, for the frequency of 20 rad/s, the movement is amplified at the top layer, therefore this frequency causes the deformation of the deposit.

Figure 10 shows the displacement time history of the top layer for the entire excitation duration. Even though the displacement time histories were plotted for all frequencies, only the plots corresponding to frequencies 20, 30, 32 and 35 rad/s are shown. In fact, these frequencies seem to clearly trace the evolution of behaviour. It can be observed that going from 20 rad/s to 30 rad/s there is an increase in the amplification of the movement; the amplitude of the top layer goes from 0.6 mm for 20 rad/s to approximately 1.6 mm for 30 rad/s. At frequencies of 32 rad/s and 35 rad/s, and in particular for the top layer but not for the other layers, the displacement plot shapes indicate the occurrence of irreversible grain sliding. This sliding could be attributed to the

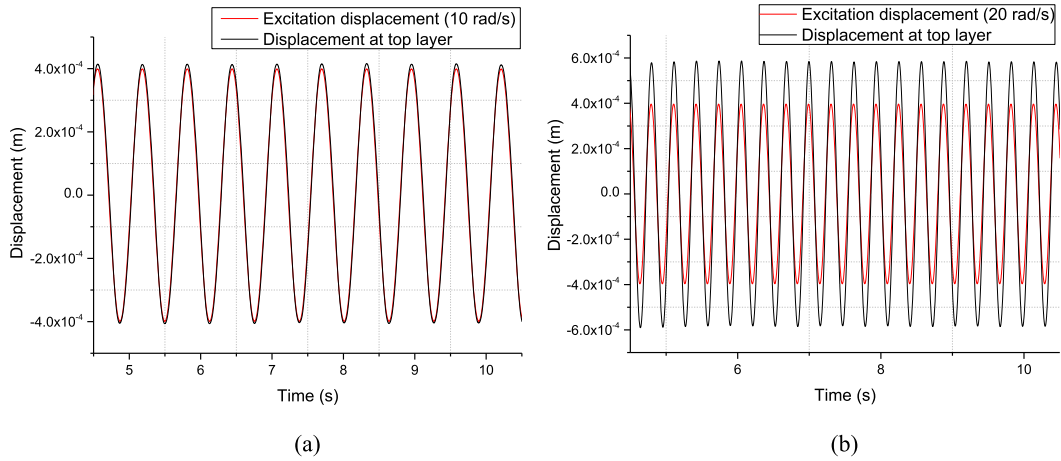


Figure 9. Steady state displacements time history at the bedrock and at the top layer of the deposit for excitation frequencies: (a) 10 rad/s, (b) 20 rad/s. Excitation amplitude $u_0 = 4 \times 10^{-4}$ m.

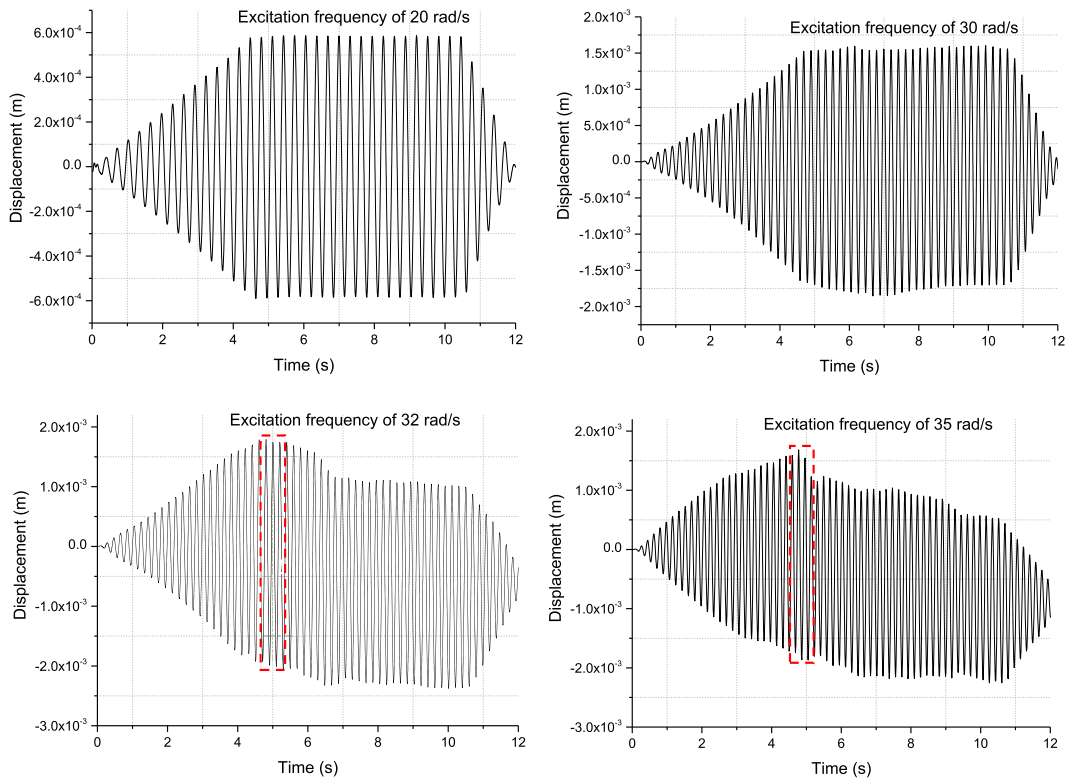


Figure 10. Time history displacements of the top layer for the excitation frequencies 20, 30, 32 and 35 rad/s. Excitation amplitude $u_0 = 4 \times 10^{-4}$ m.

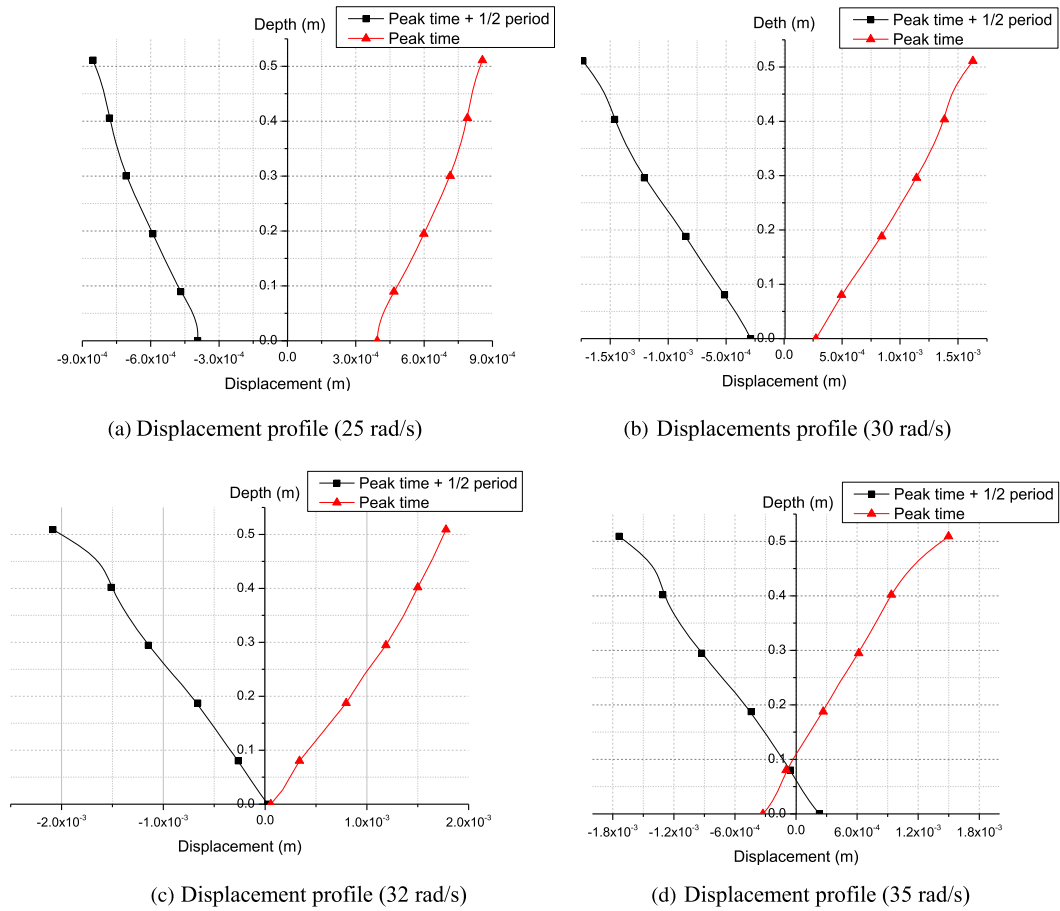


Figure 11. Displacements profiles for different excitation frequencies. Excitation amplitude $u_0 = 4 \times 10^{-4}$ m.

strong movement amplification and the non-confining of the considered layer (top layer). Note that this sliding begins when the vibration amplitude becomes sufficiently high, i.e. around the end of the excitation increasing stage. Thereafter, the layer continues to oscillate around a new position which may evolve over time. It may be noted from the plots, that the vibration amplitude tends to undergo a slight decrease with time; this behaviour may be due to the densification of the deposit which results from the significant relative movements of the grains. Note that densification leads to a reduction in the deformability of the deposit.

Meanwhile, for frequencies where top layer sliding has occurred, the steady-state vibration phase is considered to be the short phase immediately after the amplitude increase phase (i.e. after 4.5 s), it is shown in the time history displacement plots (red windows in Figure 10). This phase is shortened for these frequencies and it should correspond to the case where the sample is close to its initial state before densification. To account for the possible shift from the initial position (zero position), the amplitude of the displacement is calculated as half the difference between the maximum and minimum peak values in the taken time interval.

The displacement profiles (i.e. the deformation shape of the deposit at a given time) for the different excitation frequencies are represented in Figure 11 for the steady state vibration at a positive peak time and the next negative peak time (positive peak time + a half period).

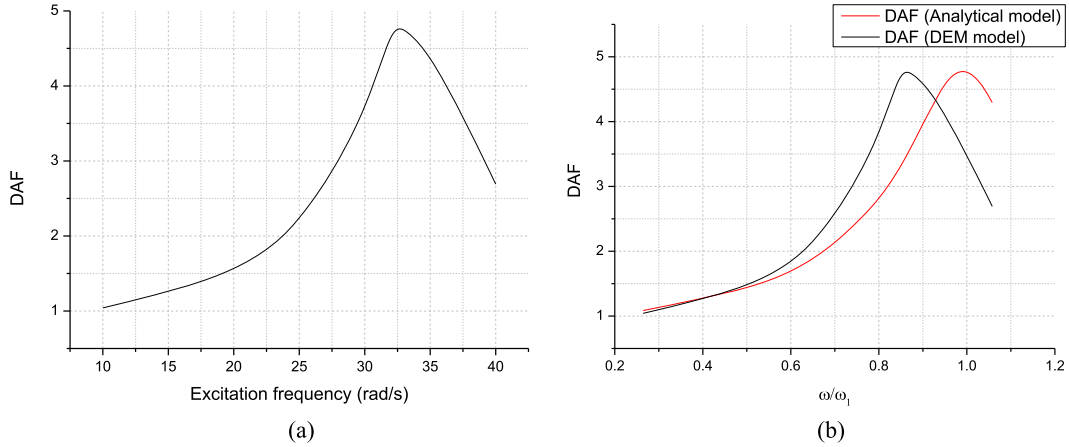


Figure 12. Dynamic Amplification Factor versus excitation frequency for excitation amplitude $u_0 = 4 \times 10^{-4}$ m. (a) DAF obtained from numerical modelling. (b) DAF comparison between numerical modelling and analytical solution.

This figure demonstrates that for low frequencies (up to 30 rad/s), the displacement profiles have the shape of the first vibration mode. For the frequency of 32 rad/s, we notice the appearance of the node with zero displacement at the base then it rises for the frequency of 35 rad/s. According to the relative discussion in Section 2, this indicates reaching and then exceeding the first resonant frequency. These shapes of displacement profiles indicate that the first resonance frequency for the excitation amplitude $u_0 = 4 \times 10^{-4}$ m, is around 32 rad/s.

We define in the following the dynamic amplification factor (DAF) at the top layer in the steady state vibration phase as:

$$\text{DAF} = \frac{u_s}{u_0} \quad (12)$$

where u_s denotes the displacement amplitude at the top layer (surface layer) and u_0 is the displacement amplitude at the bedrock (excitation).

In order to show the evolution of the amplification with frequency, the DAF as defined here is represented in Figure 12a in terms of the excitation frequency.

Figure 12a shows that the DAF evolves in a similar way to the case of an elastic deposit excited by a harmonic displacement at the base; with the increase of the excitation frequency, the DAF increases up to a maximum value that corresponds to the resonance then it decreases. The resonance frequency that can be estimated from this graph is around 32 rad/s, which agrees well with the displacement profiles in Figure 11.

For a comparison with the analytical solution, Figure 12b shows the evolution with frequency of the DAF obtained numerically and that calculated from the analytical solution presented above. The data used in this solution are those corresponding to the numerical deposit, namely $h = 0.54$ m and $\omega_1 = 37.82$ rad/s. The damping ratio is chosen so that the maximum value (at resonance) is equal to that obtained from the numerical model which is approximately $\text{DAF}_{\max} = 4.75$. Using the equation $\text{DAF}_{\max} \approx 2/\pi\xi$, we obtain the damping ratio $\xi = 13.4\%$. In this figure, the excitation frequencies are normalized by the fundamental frequency of model ω_1 . This figure shows that the evolution of the numerically computed DAF is very similar to that of the analytical solution. However, resonance occurs at a frequency about 13% lower. We believe that this difference can be attributed mainly to the degradation of the shear modulus due to the increase in shear strains near resonance.

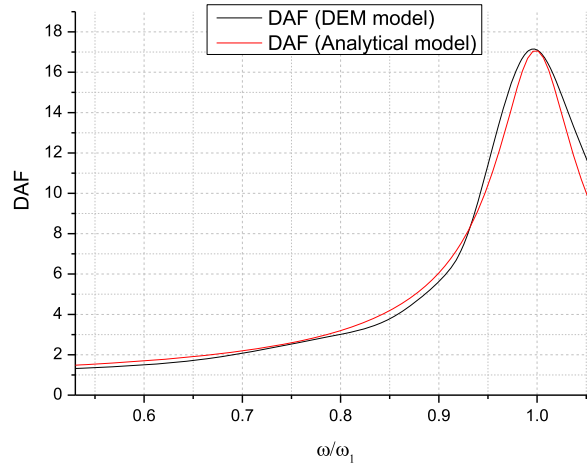


Figure 13. Dynamic Amplification Factor versus excitation frequency for excitation amplitude $u_0 = 4 \times 10^{-6}$ m. DAF obtained from numerical modelling and analytical solution.

The analysis of the effect of excitation frequency on deposit response is repeated with an excitation amplitude of $u_0 = 4 \times 10^{-6}$ m in the same way as for the amplitude 4×10^{-4} m. It is observed that for all frequencies, there is no sliding of the surface layer, and that the movement remains harmonic and regular for all layers and frequencies. The plot of the displacement profiles showed that the resonance frequency increases to around 37.5 rad/s. For this case we present only the evolution of the DAF with excitation frequency (Figure 13), in the same way as Figure 12b.

This figure shows that the resonance frequency becomes very close to the fundamental frequency estimated in Section 5.2 ($\omega_1 = 37.82$ rad/s). In addition, the maximum dynamic amplification factor increases significantly ($DAF_{\max} = 17.08$). These results indicate that there is almost no degradation of the shear modulus and that the damping ratio becomes very low for small amplitudes. We believe that the damping rate depends on intergranular slippage, which decreases with decreasing excitation amplitude. It can therefore be concluded that the resonance frequency depends on the excitation amplitude.

5.4. Influence of the excitation amplitude on the movement amplification

It should be remembered that for an elastic deposit excited at the bottom by a harmonic displacement, the *FAD* is independent of the amplitude of the excitation. However, as the granular deposit does not behave elastically in all situations, it becomes interesting to show how it behaves for different excitation amplitudes. For this purpose, simulations of the deposit response under harmonic excitation at fixed frequency (25 rad/s) and with amplitudes ranging from 2×10^{-6} m to 1×10^{-3} m are carried out. For all simulations, the displacements in the steady-state phase are plotted and the DAF as defined above is calculated.

Figure 14 shows the evolution of the DAF with the excitation amplitude. In this plot, the logarithmic scale is used for the *x*-axis (amplitudes) given the wide range of amplitude values.

It is clear that unlike the case of an elastic deposit where the DAF is theoretically constant, for the present granular deposit the DAF is almost constant for small amplitudes, but it increases sharply for large excitation amplitudes. This behaviour could be attributed to the degradation of the shear modulus due to the increase of the shear strain level when the amplitude increases. In order to check this presumption, we were interested in evaluating the shear strain level involved for the different excitation amplitudes. Observing that the displacement profile has

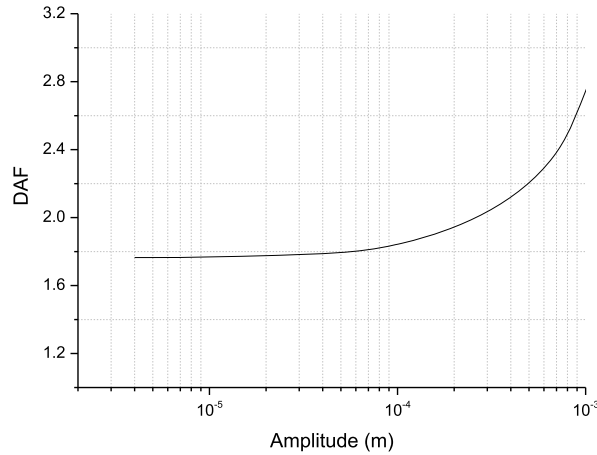


Figure 14. Evolution of the DAF at the top layer versus excitation amplitude. Excitation frequency 25 rad/s.

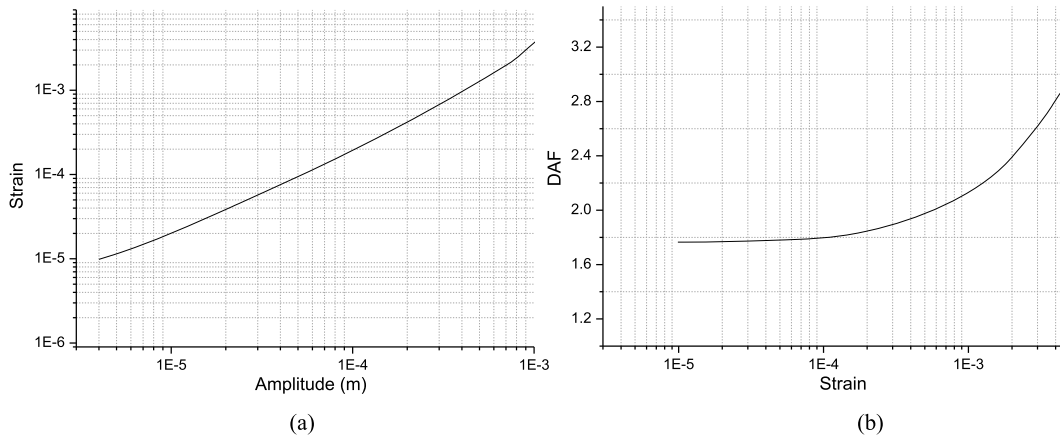


Figure 15. (a) Average shear strain level versus excitation amplitude. (b) DAF versus the shear strain level involved by the different excitation amplitudes.

an almost linear shape for the used excitation frequency (25 rad/s) as shown in Figure 11, the shear strain level (γ_0) can be approximated by the ratio of the difference between the horizontal displacements of two layers to the vertical distance between them. In order to obtain an average value over the whole deposit, γ_0 is calculated in the following using the penultimate layer (layer 9) and the first layer. Considering the possible phase shift (even very small) between the displacements of the layers, γ_0 is expressed as:

$$\gamma_0 = \frac{u_9^p - u_1}{y_9 - y_1} \tag{13}$$

where u_9^p denotes a peak displacement of layer 9, u_1 denotes displacement of layer 1 at the same time (corresponding to u_9^p) and y_i is the vertical coordinate of the i layer's center. Average shear strain levels are calculated for all the excitation amplitudes. Figure 15a shows the evolution of the shear strain level with the excitation amplitude, while Figure 15b shows the DAF versus the shear strain level involved by the different excitation amplitudes.

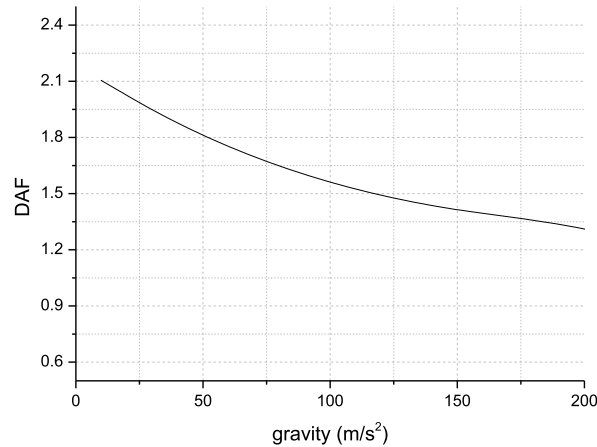


Figure 16. Evolution of the DAF with the increase of the gravity acceleration.

Figure 15a shows that the shear strain level increases monotonically (almost linearly) with increasing excitation amplitude. Taking into account the shear modulus degradation with the shear strain level curve (Figure 7b), this increase reveals that the shear modulus of the deposit decreases with the increase of the excitation amplitude, which leads to a change in the DAF. Such a change is well demonstrated by Figure 15b, this later shows that the DAF increases very slightly for small deformations, while it takes on an increasingly significant variation slope for large strains. This aspect is very similar to the shear modulus degradation curve. Furthermore, the strain threshold which separates the two phases of variation of the DAF agrees well with that which can be drawn from the degradation curve of the shear modulus (Figure 7b), it is about 10^{-4} . This result indicates that for a granular deposit, the movement can be largely amplified even when far from the fundamental frequency. This is due to the degradation of the shear modulus, which degrades with increasing excitation amplitude.

5.5. *Effect of the confining on the movement amplification*

When a layer of granular soil is deep and subjected to the weight of the upper layers, it becomes confined and its motion transmission properties change. This section aims to highlight the effect of confinement on the amplification of movement at the free surface of a granular deposit excited at its base. A simple way to simulate confinement is to increase the gravity acceleration, so in this work we analyzed the evolution of the DAF for gravity accelerations ranging from g up to $20g$. The properties of the model are the same as those presented above and the base excitation is harmonic with an amplitude of 0.4 mm and a frequency of 25 rad/s .

Figure 16 shows the evolution of the DAF as defined above, with the increase of the gravity acceleration in (m/s^2).

It is clear that the increase in the gravity acceleration decreases the amplification of the displacement at the free surface. Indeed, increasing gravity leads to an increase in effective stresses and therefore more frictional forces and less sliding, which makes the granular deposit more rigid and therefore reduces the amplification of surface movement. It can be noted that the DAF tends towards unity for large values of gravitational acceleration. This result agrees with theoretical knowledge according to which very stiff deposits (like rocks) do not amplify seismic movements.

6. Conclusion

This work consisted of a numerical analysis of the vertical propagation of shear waves in a sand deposit through 2D discrete elements modeling. The used discrete element model is based on the molecular dynamics method with circular shaped elements. The intergranular normal forces at contacts are calculated through a linear viscoelastic law while the tangential forces are calculated through a viscoelastic perfectly plastic model. Rolling friction is incorporated to account for the damping of the grains rolling motion. The exciting motion is introduced through the deposit's base (bedrock), the deposit's upper surface is free and periodic boundaries are implemented on lateral boundaries. The used excitation is harmonic with variable frequencies and amplitudes. Qualitatively, the simulations carried out highlighted some behavioral aspects of the vibration of non-cohesive deposits, such as the shape of the vertical displacement profile and the large displacements near the resonance. In the quantitative aspect, first the deposit's fundamental frequency is obtained from the free vibration at low amplitudes. Thereafter, the analysis of the effect of the excitation frequency on the response of the deposit showed in the range of the studied frequencies, that the Dynamic Amplification Factor (DAF) increases starting from 1 for low frequencies, it reaches a maximum value at the first resonance frequency then it decreases. This analysis was used to estimate the resonance frequency. It appeared that the latter is close to the fundamental frequency for low excitation amplitudes, but becomes smaller as the excitation amplitude increases. This finding may be mainly due to the degradation of the shear modulus as shear strains increase with increasing excitation amplitude. Unlike elastic deposits where the DAF is theoretically insensitive to the amplitude, the analysis of the effect of excitation amplitude on motion amplification confirmed that for a granular deposit, the DAF increases with increasing excitation amplitude. It has been shown that this behavior is due to the degradation of the shear modulus following the increase in shear strain. Furthermore, it is found that the strain threshold beyond which degradation becomes significant is in the order of 10^{-4} . Finally, the analysis of the confinement effect on the response of the deposit, is carried out by increasing the gravitational acceleration. It is shown that increasing the confinement makes the granular deposit stiffer and reduces the movement amplification at the free surface.

Ethical Approval

Not applicable.

Declaration of interests

The authors do not work for, advise, own shares in, or receive funds from any organization that could benefit from this article, and have declared no affiliations other than their research organizations.

Authors' contributions

All authors participated equally in all aspects of the study, including modeling, writing, and reviewing the manuscript.

Availability of data and materials

The authors declare that the data supporting the findings of this study will be made available on reasonable request.

References

- [1] M. H. Sadd, G. Adhikari and F. Cardoso, "DEM simulation of wave propagation in granular materials", *Powder Technol.* **109** (2000), no. 1–3, pp. 222–233.
- [2] J. F. Peters and M. Muthuswamy, "Characterization of force chains in granular material", *Phys. Rev. E* **72** (2005), article no. 041307.
- [3] C. S. Campbell, "A problem related to the stability of force chains", *Granul. Matter* **5** (2003), pp. 129–134.
- [4] N. Zamani and U. El Shamy, "Analysis of wave propagation in dry granular soils using DEM simulations", *Acta Geotech.* **6** (2011), pp. 167–182.
- [5] Z. Ning, A. Khoubani and T. M. Evans, "Shear wave propagation in granular assemblies", *Comput. Geotech.* **69** (2015), pp. 615–626.
- [6] J. O'Donovan, E. Ibraim, C. O'sullivan, et al., "Micromechanics of seismic wave propagation in granular materials", *Granular Matter* **18** (2016), article no. 56.
- [7] M. I. Arran, A. Mangeney, J. De Rosny and R. Toussaint, "Simulated slidequakes: Insights from DEM simulations into the high-frequency seismic signal generated by geophysical granular flows", *J. Geophys. Res. Earth Surf.* **129** (2024), no. 8, article no. e2023JF007455.
- [8] M. I. Arran, A. Mangeney, J. De Rosny, M. Farin, R. Toussaint and O. Roche, "Laboratory landquakes: Insights from experiments into the high-frequency seismic signal generated by geophysical granular flows", *J. Geophys. Res. Earth Surf.* **126** (2021), no. 5, article no. e2021JF006172.
- [9] V. Bachelet, A. Mangeney, R. Toussaint, J. de Rosny, M. I. Arran, M. Farin and C. Hibert, "Acoustic emissions of nearly steady and uniform granular flows: A proxy for flow dynamics and velocity fluctuations", *J. Geophys. Res. Earth Surf.* **128** (2023), no. 4, article no. e2022JF006990.
- [10] L. Fu, S. Zhou, Y. Zheng and L. Zhuang, "Characterizing dynamic load propagation in cohesionless granular packing using force chain", *Particuology* **81** (2023), pp. 135–148.
- [11] H. Nakase, T. Takeda and M. Oda, "A simulation study on liquefaction using DEM", in *Proceedings of the 2nd International Conference on Earthquake Geotechnical Engineering, Lisboa, Portugal*, 1999, pp. 637–642.
- [12] M. Jiang, A. Kamura and M. Kazama, "Numerical study on liquefaction characteristics of granular materials under Rayleigh-wave strain conditions using 3D DEM", *Soils Found.* **62** (2022), article no. 101176.
- [13] J. Cui, F. Men and X. Wang, "Soil liquefaction induced by Rayleigh wave", in *13th World Conference on Earthquake Engineering, Vancouver, B.C., Canada, August 1–6, 2004*.
- [14] P. A. Cundall and O. D. Strack, "A discrete numerical model for granular assemblies", *Géotechnique* **29** (1979), no. 1, pp. 47–65.
- [15] P. A. Cundall and R. D. Hart, "Numerical modelling of discontinua", *J. Eng. Comput.* **9** (1992), pp. 101–113.
- [16] V. Richefeu, *Approche par éléments discrets 3D du comportement de matériaux granulaires cohésifs faiblement contraints*, Thèse, Université Montpellier II - Sciences et Techniques du Languedoc, 2005. Français. NNT: tel-00012112.
- [17] T. Pöschel and T. Schwager, *Computational Granular Dynamics - Models and Algorithms*, Springer-Verlag, Berlin, Heidelberg, 2005.
- [18] M. Mansouri, M. S. El Youssoufi and F. Nicot, "Numerical simulation of the quicksand phenomenon by a 3D coupled Discrete Element - Lattice Boltzmann hydromechanical model", *Int. J. Numer. Anal. Meth. Geomech.* **41** (2017), no. 3, pp. 338–358.
- [19] D. Saidani, M. Mansouri and A. Khellaf, "Analysis of the preloading effect on shear strength for dense sandy soils A discrete element modeling", *Innov. Infrastruct. Solut.* **7** (2022), article no. 81.
- [20] A. Verruijt, *An Introduction to Soil Dynamics*, Springer, Dordrecht, Heidelberg, London, New York, 2010.
- [21] French Committee of Soil Mechanics and Geotechnical Engineering, CFMS, *Recommendations for Numerical Modeling of Geotechnical Structures*, Centre Français d'exploitation du droit de copie, Paris, 2023.